Molecular Physics

An International Journal at the Interface Between Chemistry and Physics

ISSN: 0026-8976 (Print) 1362-3028 (Online) Journal homepage: https://www.tandfonline.com/loi/tmph20

Quantum Monte Carlo assessment of density functionals for π-electron molecules: ethylene and bifuran

Egor Ospadov, Stuart M. Rothstein & Roi Baer

To cite this article: Egor Ospadov, Stuart M. Rothstein & Roi Baer (2019) Quantum Monte Carlo assessment of density functionals for π-electron molecules: ethylene and bifuran, Molecular Physics, 117:17, 2241-2250, DOI: 10.1080/00268976.2018.1517905

To link to this article: https://doi.org/10.1080/00268976.2018.1517905

MOLECULAR PHYSICS
2019, VOL. 117, NO. 17, 2241–2250
https://doi.org/10.1080/00268976.2018.1517905

Taylor & Francis
Taylor & Francis Group

58TH SANIBEL SYMPOSIUM

Quantum Monte Carlo assessment of density functionals for π-electron molecules: ethylene and bifuran

Egor Ospadov[a], Stuart M. Rothstein[b] and Roi Baer[c]

[a]Department of Chemistry, The University of Western Ontario, London, ON, Canada; [b]Department of Physics, Brock University, St. Catharines, ON, Canada; [c]Fritz Haber Center for Molecular Dynamics and Institute of Chemistry, The Hebrew University of Jerusalem, Jerusalem 9190401, Israel

ABSTRACT

We perform all-electron, pure-sampling quantum Monte Carlo (QMC) calculations on ethylene and bifuran molecules. The orbitals used for importance sampling with a single Slater determinant are generated from Hartree-Fock and density functional theory (DFT). Their fixed-node energy provides an upper bound to the exact energy. The best performing density functionals for ethylene are BP86 and M06, which account for 99% of the electron correlation energy. Sampling from the π-electron distribution with these orbitals yields a quadrupole moment comparable to coupled cluster CCSD(T) calculations. However, these, and all other density functionals, fail to agree with CCSD(T) while sampling from electron density in the plane of the molecule. For bifuran, as well as ethylene, a correlation is seen between the fixed-node energy and deviance of the QMC quadrupole moment estimates from those calculated by DFT. This suggests that proximity of DFT and QMC densities correlates with the quality of the exchange nodes of the DFT wave function for both systems.

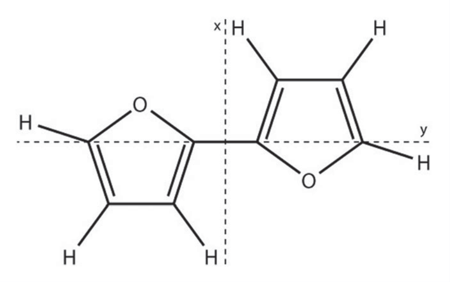

ARTICLE HISTORY
Received 26 April 2018
Accepted 20 August 2018

KEYWORDS
Density functional theory; quadrupole moment; ethylene; bifuran; pure-sampling quantum monte carlo

1. Introduction

A recent paper by Medvedev et al. [1] examined root mean squared deviations of electron densities for several atomic systems calculated using various density functionals relative to highly accurate wave function calculations. They found that for more recent, highly parameterised density functionals, the density becomes less accurate while the energy grows more accurate. The recently developed functionals started producing less accurate electron densities following early generalised gradient approximation (GGA) methods. Their paper has led to much discussion in the literature on whether or not density functional theory (DFT) has been on the 'wrong track' since early 2000, after highly parameterised density functionals came into prominence.

The methodology used by Medvedev et al. has been questioned repeatedly. Kepp [2] points out that their calculations were performed on very compact $1s^2$ and $1s^2 2s^2$ systems favoured by the Hartree-Fock model and irrelevant to chemical bonding. Medvedev et al. [3] replied that nevertheless this does not change the main message of their work: unconstrained fitting of flexible functional forms can make the model less widely predictive. In the same vein, Mezei et al. [4] addressed the same methodological bias by preforming a propagation of error analysis for the density, its gradient, and its Laplacian for a set of chemically relevant densities. Although the details of their conclusions are different, they nonetheless confirm the broad conclusions stated by Medvedev et al.

CONTACT Stuart M. Rothstein srothste@brocku.ca Department of Physics, Brock University, St. Catharines, ON L2S3A1, Canada

Some recent papers also question the accuracy of highly parameterised density functionals. As a follow-up to her comments in Science [5], Hammes-Schiffer and co-workers [6] calculated the errors relative to couple cluster (CCSD) reference calculations in the electron densities and atomisation energies in the bonding region for a series of diatomic molecules using 90 different density functionals. They found that these errors are uncoupled for hybrid GGA functionals developed since year 2000: the accuracy of the energies remains relatively consistent while the accuracy of the densities varies significantly. In the analysis of the electron density of beryllium atom, relative to CCSD reference calculations, Korth [7] found M06, one of the recently developed functionals, to be less accurate than PBE0, despite using more parameters. M06 and M06L (another recently developed functional) appeared with eleven others in Kepp's study of bond enthalpies for systems containing aluminium. In terms of their ability to reproduce trends in bond strengths, all methods except M06 and M06L performed equally well. He concluded that the accuracy of heavily parameterised functionals may suffer when applied outside of their parametrisation range.

On the other hand, there are impressive results from benchmarks covering a wide variety of computational chemistry applications performed with the non-local members of the M06 suite of functionals [8]. On thermochemistry, barrier heights, non-covalent interaction energies and (albeit now omitting M06-SCF) transition metal reaction energies, these functionals outperform BLYP, B3LYP, PBE, PBE0 and TPSSh, most of the functionals being assessed in the present study.

We add to this discussion by applying all-electron, pure-sampling quantum Monte Carlo (PSQMC) to ethylene and bifuran. Ethylene, a small molecule of obvious importance, is amenable to an all-electron approach, promising acceptably small error bars for quantities of interest to us. As to be expected, similar calculations on bifuran, a conducting polymer oligomere, result in larger error bars. Nevertheless, for our purposes, the statistical error is sufficiently small for us to draw some meaningful conclusions from our results.

For importance sampling, we employ a single-determinant of molecular orbitals generated using Hartree-Fock and a variety of density functionals. Given physically meaningful orbitals, the resulting fixed-exchange-node energy provides an upper bound on the exact, non-relativistic, Born-Oppenheimer ground-state energy. A correlation is seen between the fixed-node energy and deviance of the PSQMC quadrupole moment estimates from those calculated by DFT. This suggests that proximity of the DFT and PSQMC densities correlates with the quality of the exchange-nodes of the Slater determinental wave function. This gives us an objective way to assess the quality of the underlying ground-state electron distributions, as reflected by their electric quadrupole moments, without relying on a favourable cancellation of errors inherent in, for example, thermochemistry calculations, reaction barrier heights and bond energies. Furthermore, our approach does not rest on such rubrics as clever definitions of bonding regions or an analysis of electron density along a covalent bond. Instead, pure-sampling quantum Monte Carlo samples literally millions of times from the entire, exact, save for its inexact electron-exchange nodes, electron density distribution.

2. Methods

2.1. Pure-sampling quantum monte carlo

Pure-sampling algorithms are designed to calculate electronic properties that are free from importance-sampling bias. We employ the most recent algorithm of this type, denoted as pure-sampling quantum Monte Carlo (PSQMC) [9,10], which uses special techniques that remove not only the importance-sampling bias, but also more subtle problems associated with other approaches, such as fixed-node diffusion Monte Carlo (FN-DMC) [11–13], reptation quantum Monte Carlo [14,15] and 'bounce' quantum Monte Carlo [16]. For a detailed review of these methods and their associated biases and other technical issues, see Reference [17].

All of these algorithms, including PSQMC, rest upon the fixed-node approximation; described in Section 2.2. The resulting fixed-node bias is a variationally bound quantity that is generally believed to be a small percentage of the correlation energy. Nevertheless, it could still lead to difficulties with calculating small energy differences [18] and spin densities [19].

Most of the literature with applications of density functional theory in consort with quantum Monte Carlo calculations utilises FN-DMC. Several of these have incorporated density functional wave functions for the importance-sampling [18–34]. However, relatively few exploit pure-sampling to analyse the performance of density functionals for properties other than the energy, either by using extrapolation [23,32,35–37] or reptation-based algorithms [22,26,38]. Extrapolation has a bias proportional to the square of the error in the importance-sampling function [39]. Reptation algorithms, reviewed in [40], have no such bias, but assume microscopic reversibility, the failure of which may have adverse consequences for pure-sampling [10]. All-electron calculations are relatively rare in the literature, for example [21,25,27,28,32]. Discussions of the pseudopotential approximation and its impact on their FN-DMC results appear in [18,22,36,41–43].

PSQMC is not affected by these biases and theoretical limitations, presenting itself as an ideal method to study the quality of the ground-state electron distributions.

2.2. The algorithm

Pure-sampling quantum Monte Carlo (PSQMC) carries out a random walk in tiny increments of imaginary time (time-step), τ, to generate the τ-biased mixed-distribution of elections, $\Psi\Phi_0$, and their pure distribution, Φ_0^2. Here Ψ is an inputted antisymmetric wave function, which is used for importance-sampling, and Φ_0 is the unknown, 'exact' ground-state wave function. Φ_0 is not truly exact, as its electron-exchange nodes are fixed to agree with those provided by Ψ. This rubric is the so-called 'fixed-node approximation' [11], which introduces a positive bias on the calculated energy. (It is important for the reader not to confuse the 3N-dimensional electron-exchange nodes (N electrons) for the spatial nodes in atomic and molecular orbitals.) Similarly, averaging over the pure distribution of electrons with operators that commute with the position operator yields properties like the electrical moments, albeit, still τ- and fixed-node-biased. These τ-biases are easily eliminated by regression to zero time-step, but the fixed-node biases remain.

The calculations start with a random (or variational, or other suitably chosen) electron configuration: 3N coordinates of the N electrons, denoted by x_0 in Figure 1.

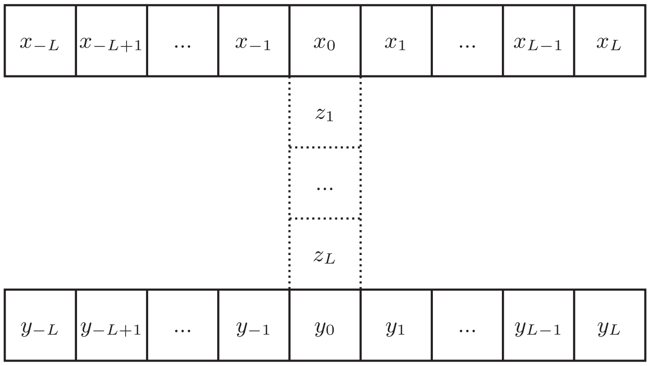

Figure 1. Visual representation of the process used to generate **X** and **Y** in our methodology. Path **X** is generated from x_0. The auxiliary path **Z** is generated starting from x_0 as well. Finally, path **Y** is generated starting from z_L. All the moves are done using drift and diffusion (Langevin diffusion). For the sake of illustration, the paths are shown running in either the vertical or horizontal direction. They can actually go in any direction and may even cross each other. Reprinted from [9] with permission of AIP Publishing.

Starting from x_0, after employing a series of drift and diffusion moves:

$$x_{i+1} = x_i + \tau \frac{\nabla\Psi(x_i)}{\Psi(x_i)} + \sqrt{\tau}\chi, \tag{1}$$

one generates Paths **X** and **Y**, each with $2L+1$ configurations, and auxiliary Path **Z**, with L configurations. χ in Equation (1) is a random draw from a 3N-dimensional standard normal distribution, performed each time these mathematical moves (with no physical significance) are executed. Next, a Metropolis decision,

$$\mathrm{A}(\mathbf{X} \to \mathbf{Y}) = \min\left\{\mathbf{1}, \mathrm{e}^{[\mathbf{S(X)}-\mathbf{S(Y)}]}\right\}, \tag{2}$$

is evoked, where Path **Y** is considered as a proposed path and Path **X** is the current path. S is the sum of local energies,

$$\mathrm{E}_{\mathrm{loc}} = \mathbf{H}\Psi/\Psi, \tag{3}$$

along the indicated Path, with double counting the local energy evaluated at the middle of the Path.

$$\mathrm{S}(\mathbf{X}) = \tau\left[\frac{1}{2}\mathrm{E}_{\mathrm{loc}}(x_{-L}) + \sum_{i=-L+1}^{L-1}\mathrm{E}_{\mathrm{loc}}(x_i) + \mathrm{E}_{\mathrm{loc}}(x_0) + \frac{1}{2}\mathrm{E}_{\mathrm{loc}}(x_L)\right]; \tag{4}$$

S(**Y**) is analogously defined.

After this procedure has equilibrated, if the proposed path is accepted, its middle configuration, y_0, is a random sample drawn from the time-step-biased pure distribution, $\Phi_0{}^2$, and the proposed path becomes the current one in the next iteration. Otherwise, the middle of the current path, x_0, is a random draw from this distribution and retained for the next iteration, when new Paths **Y** and **Z** are generated. The time-step-biased mixed distribution, $\Psi\Phi_0$, is sampled at the end configurations on the accepted path.

The local energy, Equation (3), is sampled from the mixed distribution at every time-step, providing the fixed-node energy after the extrapolation to zero time-step. Similarly, the electric quadrupole moment estimators:

$$\Theta_{\alpha\beta} = \frac{1}{2}\sum_i q_i\left(3r_{i\alpha}r_{i\beta} - r_i^2\delta_{\alpha\beta}\right), \tag{5}$$

are averaged over the pure distribution, at the middle of the Metropolis-selected path, and these time-step biased quantities are also extrapolated to zero τ. The above sum is taken over all electrons, and the Greek letters are Cartesian coordinates.

Since they are separated by an auxiliary Path **Z**, Paths **X** and **Y** are effectively statistically independent of each other, and the Metropolis decision, Equation (2), is valid without approximations. By virtue of this 'independent Metropolis' [10], extrapolating the Monte Carlo estimators to zero τ is easier and more reliable.

2.3. Truncations and path-lengths

We employ τ-dependent truncations to avoid detrimental numerical issues that arise from singularities affecting the Langevin diffusion moves, Equation (1), and local energy, Equation (3). The truncations, which are rarely evoked in practice and detailed in the literature [9,44], are unbiased in the limit as $\tau \to 0$, where the fixed-node values of the properties are determined and the underlying short-time Green's function is free from bias [45–47].

The calculations are carried out at various time-steps and path-lengths:

$$L(\tau) = L_0 \times \left(\frac{\tau_0}{\tau}\right), \tag{6}$$

where L_0 is the initial (smallest) path-length and τ_0 is the initial (largest) time-step. The path-length (L) approaches to infinity as τ tends to zero.

2.4. Biases

The algorithm is repeated for a set of τ values, and the data set is fit by a polynomial (or exponential) variance-weighted regression. This eliminates the time-step bias in the simulated quantities. Nevertheless, due to the choice of regression model, the desired zero-τ intercept is still biased!

To deal with the regression model bias, several energy versus τ curves are generated, where the length of Paths **X** - **Z** is systematically increased until the fixed-node energy and other properties converge to statistically equivalent values at zero time-step. These are weighted-averaged to improve the precision of the final determination of these quantities. At some point, for well-understood reasons, described in detail in [9], the curves assume an 'S-shape' and cannot be fit by any reasonable regression model. This signals that the paths are too long.

Importance sampling reduces the statistical error that is inherent in Monte Carlo sampling of configuration space. In our case, this is provided by Ψ, a single-determinant wave function with molecular orbitals coming from Hartree-Fock and a variety of density functional calculations performed by using Amsterdam Density Functional (ADF) [48,49] software.

Variance reduction is done at the cost of Ψ's unoptimised and fixed electron-exchange nodes being forced upon the simulated electron distributions, thereby biasing quantities of interest to us. This so-called fixed-node approximation [11] introduces a positive bias on the calculated energy. The fixed-node bias is fundamental to PSQMC and Reptation Quantum Monte Carlo [14,15], its nearest alternative in the literature.

Biases that are *not* present in these calculations include:

1. pseudopotential approximation: these calculations are all-electron.
2. population control bias: present in the well-used, FN-DMC method , but absent with PSQMC.
3. finite path-lengths: the path-lengths are infinite at zero time-step, where the fixed-node energy and other properties are evaluated; Equation (6).
4. Metropolis decision: Equation (2) is exact.

Relativity is ignored. The nuclei are clamped at their experimental (ethylene) or energy-optimised (bifuran) geometry. Our calculations are subject to the fundamental fixed-exchange-node bias and limitations of single reference importance sampling with a finite (yet large) STO basis set.

3. Application to ethylene

In the first instance, we applied the PSQMC algorithm to ethylene. Using Amsterdam Density Functional (ADF) [48,49] software, we constructed a Hartree-Fock single-determinant of molecular orbitals. The molecular orbitals were expressed in a QZ4P basis set of Slater-type orbitals (194 atomic orbitals) at the experimental geometry [50]. Next, we determined the effective range of time-steps and the path-length parameter, L_0, at the largest time-step, τ_0, with which to do our calculations. (The path-length L increases as the time-step decreases, approaching to infinity as the time-step approaches to zero; see Equation (6).) The fixed-node values and associated error bars for the components of the electric quadrupole moment and the energy are drawn from the zero time-step intercept from a variance-weighted regression of their time-step-biased quantities. These calculations were repeated as L_0 was systematically increased until the resulting data could not be fit by regression. At that point, a variance weighted average was taken over statistically equivalent fixed-node energies and components of the electric quadrupole moment. These quantities, with HF importance sampling, comprise the 'HF' entry in Table 1.

The following set of density functionals was selected for importance sampling, again with a single-determinant of molecular orbitals expanded in a QZ4P basis set: BHandH [51,52], TPSS [53], TPSSh [54,55], M06-L [56], PBE0 [57,58], B3LYP [52,59,60], PBE [61], BLYP [52,62],

Table 1. Fixed-node energy (E_{FN}) and electric quadrupole moment components for ethylene, generated by pure-sampling quantum Monte Carlo, with importance sampling provided by a single-determinant of hartree-Fock (HF) and density functional orbitals.

WFN	Type (year)	%X	E_{FN}	Q_{xx}^{FN}	Q_{yy}^{FN}	Q_{zz}^{FN}	Trace[a]
BLYP	GGA (1988)	0	−78.574 (4)	−2.485 (10)	1.235 (10)	1.256 (11)	0.006
BP86	GGA (1986)	0	−78.585 (3)	−2.517 (2)	1.262 (6)	1.261 (10)	0.006
M06-L	mGGA (2006)	0	−78.572 (3)	−2.429 (2)	1.185 (6)	1.243 (6)	−0.001
PBE	GGA (1996)	0	−78.578 (3)	−2.495 (6)	1.245 (7)	1.254 (8)	0.003
TPSS	mGGA (2003)	0	−78.567 (3)	−2.481 (10)	1.223 (8)	1.255 (9)	−0.003
TPSSh	h-mGGA (2003)	10	−78.570 (3)	−2.542 (10)	1.251 (8)	1.299 (13)	0.009
B3LYP	h-GGA (1994)	20	−78.578 (4)	−2.574 (12)	1.271 (13)	1.301 (12)	−0.003
PBE0	h-GGA (1995)	25	−78.574 (4)	−2.616 (8)	1.293 (7)	1.329 (10)	0.005
M06	h-mGGA (2008)	27	−78.584 (4)	−2.527 (9)	1.231 (9)	1.289 (13)	−0.007
BHandH	h-GGA (1993)	50	−78.566 (3)	−2.730 (11)	1.327 (7)	1.394 (9)	−0.009
HF		100	−78.570 (3)[b]	−2.832 (7)	1.301 (8)	1.537 (8)	0.007
CCSD (*T*)[c]			−78.58079	−2.46739	1.39787	1.06952	

Note: Energy in hartrees and quadrupole moment in atomic units. Entries in parentheses reflect statistical error in the last decimal place quoted. For geometry, see caption of Figure 4.

[a] $Q_{xx} + Q_{yy} + Q_{zz}$. Components independently calculated.

[b] Variational energy equals −78.069 Hartrees (Table 2).

[c] Reference [66].

M06 [8] and BP86 [62–64]. These calculations were performed in the same manner as the HF case, described above.

We checked the validity of our trial DFT wave functions by performing a second set of calculations which used Libxc [65] to evaluate the functionals in conjunction with ADF. Afterwards, we performed our PSQMC calculations as usual. Both sets of calculations agreed within the error bars reported by us.

The fixed-node energy and electric quadrupole moments are reported in Table 1 and displayed in Figures 2–6.

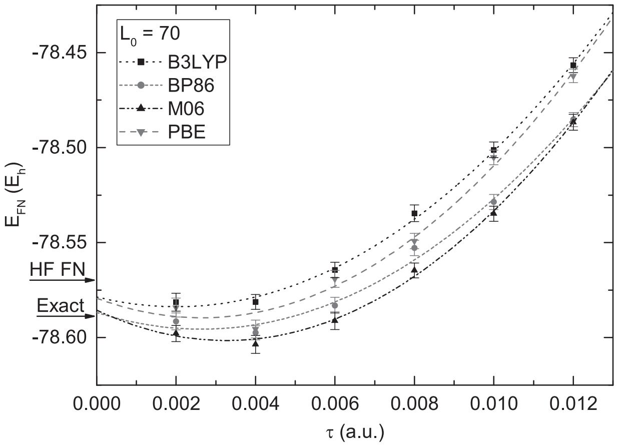

Figure 2. Plots of the time-step-biased energy versus time-step at the largest value of $L_0 = 50$. Path-lengths L increase from L_0 as the time-step decreases; Equation (6). Importance sampling is provided by density functional orbitals, in a Slater determinant, with lower fixed-node energy than Hartree Fock. The fixed-node energy for a given functional, with this choice of L_0, is the zero time-step intercept of its time-step-biased energies. Subsequently, this result is included within a variance-weighted average taken over statistically equivalent fixed-node energies, calculated with smaller L_0 values.

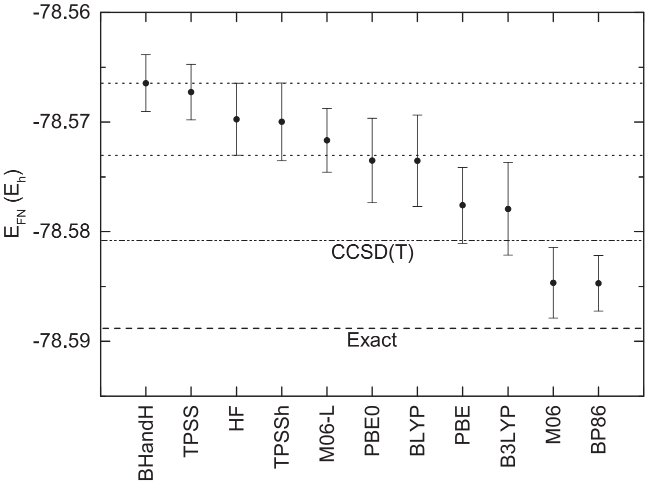

Figure 3. Fixed-node (FN) energy for ethylene ground-state calculated with importance sampling provided by a single Slater determinant constructed from Hartree Fock and density functional orbitals. The error bars are a weighted average over statistically equivalent fixed-node energies from curves generated at a number of L_0 values. The dotted lines denote the upper and lower reaches of the error bars on the Hartree-Fock fixed-node energy. The couple cluster value (CCSD(T)) was provided by [66], and the exact, non-relativistic energy is taken from [67].

The quadrupole moment components are calculated independently. The column labelled ‘trace’ in Table 1 shows that the components obey the tensor's traceless requirement comparable to the error bars of its components. The dipole moment vanishes by symmetry. The energy and quadrupole moments calculated from density functional theory are reported in Table 2.

In Figure 3, the variationally bound, fixed-node energies for B3LYP, PBE, M06 and BP86 appear below the Hartree-Fock error bars. In turn, M06 and BP86 have better fixed-node energies than B3LYP and PBE. A critical, albeit not decisive, variable is % HF exchange: the

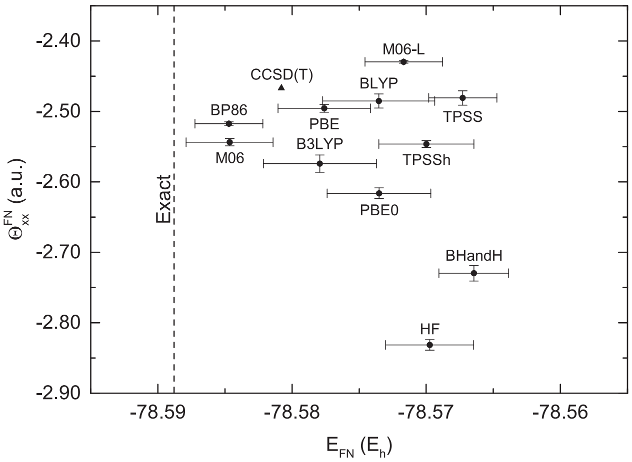

Figure 4. Purely sampled Q_{xx} electric quadrupole moment component of ground-state ethylene versus fixed-node energy, calculated with importance sampling provided by a single Slater determinant constructed from Hartree-Fock and density functional orbitals. As the fixed-node energy improves, the values converge to those calculated from M06/BP86 The experimental geometry [50] is assumed, where the *x*-axis is perpendicular to the plane of the molecule. Coordinate origin is taken at the middle of the *z*-axis, which contains the C–C bond. All PSQMC quantities are subject to the fundamental fixed-node (FN) bias. The couple cluster value (CCSD(T)) is provided by [66], and the exact, non-relativistic energy is taken from [67].

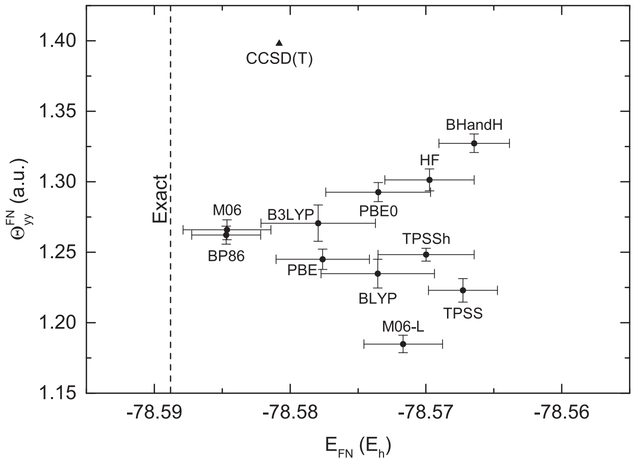

Figure 5. Purely sampled Q_{yy} electric quadrupole moment component for ethylene ground-state versus fixed-node energy. For geometry and other details, see caption of Figure 4.

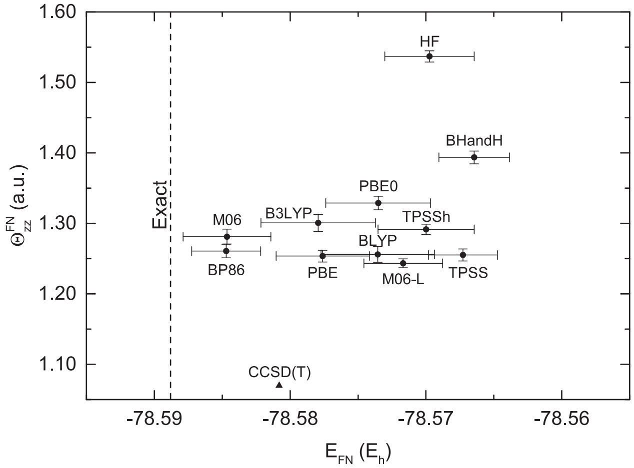

Figure 6. Purely sampled Q_{zz} electric quadrupole moment component for ethylene ground-state versus fixed-node energy. For geometry and other details, see caption of Figure 4.

worst performing, yet still valid, density functional model is BHandH with 50 % exact exchange.

The quadrupole moments converge to their BP86 and M06 values as the fixed-node energy decreases (Figures 4–6). There is a similar convergence for the error in the density: that which remains by subtracting the fixed-node quadrupole moment from its DFT-calculated value (Figures 7–9).

The CCSD(T) electric quadrupole moment determinations, quoted in Table 1 and in Figures 4–6, employed an aug-cc-pV5Z basis set on hydrogen and an aug-cc-pCV5Z basis set on carbon, 682 basis functions [66]. Q_{xx}^{FN} values calculated from BP86, M06, PBE and to a lesser extent B3LYP are in reasonable agreement with coupled cluster. It is important to remember that the π electron

Table 2. ADF-generated energy (E_{ADF}) and electric quadrupole moment components for hartree-Fock (HF) and density functional models for ethylene.

WFN	Type (year)	%*X*	E_{ADF}	Q_{xx}^{DFT}	Q_{yy}^{DFT}	Q_{zz}^{DFT}
BLYP	GGA (1988)	0	−78.584	−2.285	1.180	1.105
BP86	GGA (1986)	0	−78.626	−2.362	1.213	1.149
M06-L	mGGA (2006)	0	−77.849	−2.236	1.137	1.098
PBE	GGA (1996)	0	−78.508	−2.367	1.215	1.152
TPSS	mGGA (2003)	0	−77.853	−2.338	1.185	1.153
TPSSh	h-mGGA (2003)	10	−76.985	−2.404	1.205	1.199
B3LYP	h-GGA (1994)	20	−78.572	−2.460	1.245	1.245
PBE0	h-GGA (1995)	25	−78.521	−2.558	1.278	1.280
M06	h-mGGA (2008)	27	−77.188	−2.391	1.183	1.208
BHandH	h-GGA (1993)	50	−77.964	−2.758	1.341	1.417
HF		100	−78.069[a]	−2.849	1.317	1.532

Note: Energy in hartrees and quadrupole moment in atomic units. For geometry see caption of Figure 4.
[a] Variational energy.

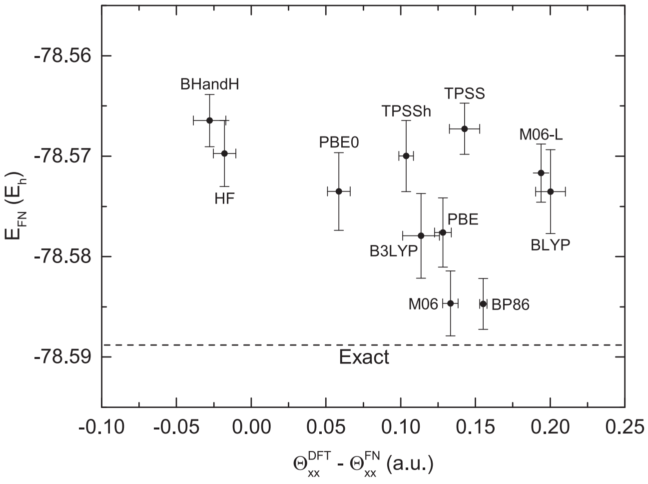

Figure 7. Fixed-node (FN) energy for ethylene ground-state calculated with importance sampling constructed from the corresponding density functional (DFT) versus $Q_{xx}^{DFT} - Q_{xx}^{FN}$. As the fixed-node energy, and hence, electron distribution improves, the error in the quadrupole moment component, based on pure-sampling, converges to those calculated from M06/BP86. For geometry, see caption of Figure 4.

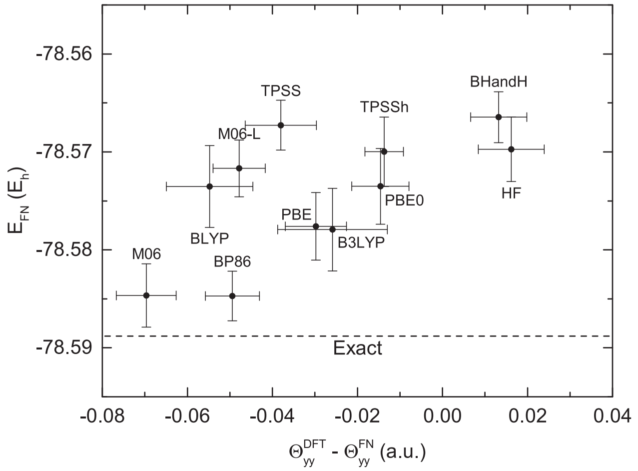

Figure 8. Fixed-node (FN) energy for ethylene ground-state calculated with importance sampling constructed from the corresponding density functional (DFT) versus $Q_{yy}^{DFT} - Q_{yy}^{FN}$. For geometry, see caption of Figure 4.

density is distributed above and below the *yz*-planes that contain the core and σ-bonded electrons. On the other hand, *none* of the density functional models are in good agreement with coupled cluster for Q_{yy} and Q_{zz}.

4. Application to 2,2′-bifuran

Our next system is bifuran. Its symmetry affords in-plane sampling similar to ethylene, where we found discrepancy in the quadrupole moment relative to CCSD(T) values. This molecule contains hetero-atoms, and unlike ethylene, bifuran is sufficiently large to present a computational challenge for an all-electron approach to pure-sampling.

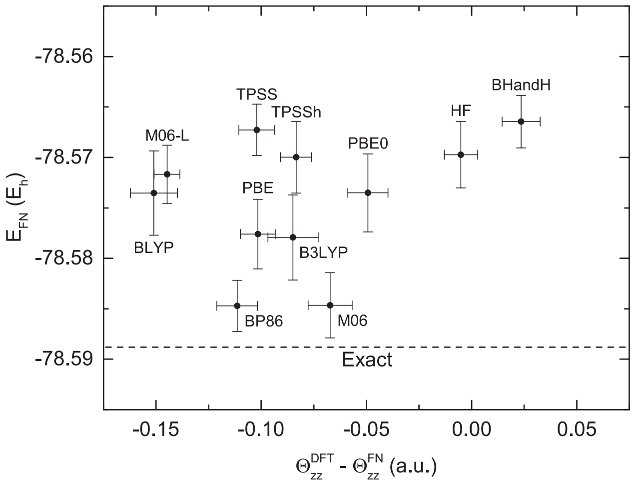

Figure 9. Fixed-node (FN) energy for ethylene ground-state calculated with importance sampling constructed from the corresponding density functional (*DFT*) versus $Q_{zz}^{DFT} - Q_{zz}^{FN}$. For geometry, see caption of Figure 4.

In this application, a single Slater determinant was again employed for importance-sampling. Here, the molecular orbitals were expressed in a TZ2P basis set of Slater-type orbitals with an energy-optimised geometry. There are 70 electrons, 16 nuclei and 372 atomic orbitals.

Again using ADF [48,49], we constructed importance-sampling functions with orbitals calculated from Hartree-Fock and density functional theory: BHandH [51,52], PBE0 [57,58], B3LYP [52,59,60], BLYP [52,62], Becke [62] and BP86 [62–64].

In Table 3, we see the most negative fixed-node energies are calculated for B3LYP, BLYP, Becke and BP86 wave functions, labelled ‘best set’ in the table, after taking into account the statistical error. Their weighted mean provides the fixed-node energy for bifuran to within 8 milli-Hartree precision. For this set of functionals, the amount of exact exchange does not exceed 20%. The variance-weighted fixed-node energy for BHandH and PBE0 is 70 milli-Hartrees more positive than that of the best performing functionals.

In Table 4, the *xx*- and *zz*-components of the electric quadrupole moment calculated from the best set differ markedly from their counterparts calculated with the other functionals. The *xy*- and *yy*-components are less sensitive to the molecule’s nodal structure. The *zz*-component, which arises from sampling the π-electron distribution, consistently has the smallest variance. The column labelled ‘trace’ shows that the quadrupole moment components, calculated independently from each other, obeys the tensor’s traceless requirement to well within the error bars on its components.

Table 3. Fixed-node energy (E_{FN}) and purely sampled electric quadrupole moment components for hartree-Fock (HF) and density functional models for bifuran.

WFN	Type (year)	%*X*	E_{FN}	Q_{xx}	Q_{xy}	Q_{yy}	Q_{zz}	Trace[a]
BLYP	GGA (1988)	0	−458.700 (31)	0.37 (14)	1.02 (17)	8.66 (22)	−9.05 (12)	−0.022
BP86	GGA (1986)	0	−458.679 (11)	0.48 (15)	1.29 (18)	8.83 (23)	−9.32 (13)	−0.005
Becke	GGA (XXX)	0	−458.669 (18)	0.07 (14)	0.82 (19)	8.80 (21)	−8.86 (12)	0.006
B3LYP	h-GGA (1994)	20	−458.705 (25)	0.26 (13)	0.81 (16)	9.07 (19)	−9.35 (11)	−0.015
PBE0	h-GGA (1995)	25	−458.633 (15)	0.69 (12)	1.31 (17)	8.79 (17)	−9.47 (10)	0.010
BHandH	h-GGA (1993)	50	−458.601 (10)	0.83 (14)	1.00 (19)	8.78 (22)	−9.63 (13)	−0.018
HF		100	−458.494 (49)[b]	0.83 (15)	1.26 (21)	8.75 (21)	−9.58 (12)	0.001
Best set[c]			−458.681 (8)	0.28 (7)	0.98 (9)	8.86 (11)	−9.14 (6)	
Others[d]			−458.611 (8)	0.75 (9)	1.17 (12)	8.79 (14)	−9.53 (8)	

Note: Energy in hartrees and quadrupole moment in atomic units. Energy-optimised geometry, where the molecule rests in the *xy*-plane. Entries in parentheses reflect statistical error in the last decimal place quoted.

[a] $Q_{xx} + Q_{yy} + Q_{zz}$. Components independently calculated.

[b] Variational energy: −456.2723 E_h.

[c] Variance-weighted average: B3LYP, BLYP, Becke and B86.

[d] Variance-weighted average: BHandH and PBE0.

Table 4. ADF-generated components of electric quadrupole moment for hartree-Fock (HF) and density functional wave functions for ground-state of bifuran.

WFN	Q_{xx}	Q_{xy}	Q_{yy}	Q_{zz}
HF	0.749	1.008	9.433	−10.183
BHandH	0.962	1.206	9.074	−10.036
PBE0	0.819	1.216	8.893	−9.712
B3LYP	0.431	1.043	8.973	−9.403
Becke	−0.005	1.072	8.673	−8.668
BP86	0.553	1.282	8.690	−9.244
BLYP	0.198	1.149	8.709	−8.907
Others[a]	0.89 [0.75 ±0.09]	1.21 [1.17±0.12]	8.98 [8.79 ±0.14]	−9.87 [−9.53 ±0.08]
Best[b]	0.29 [0.28 ±0.07]	1.14 [0.98 ±0.09]	8.76 [8.86 ±0.11]	−9.06 [−9.14 ±0.06]

Note: All values are in atomic units. For other details, see caption of Table 3.

[a] Average: BHandH and PBE0. Fixed-node average in brackets (Table 3).

[b] Average: B3LYP, BLYP, Becke and B86. Fixed-node average in brackets (Table 3).

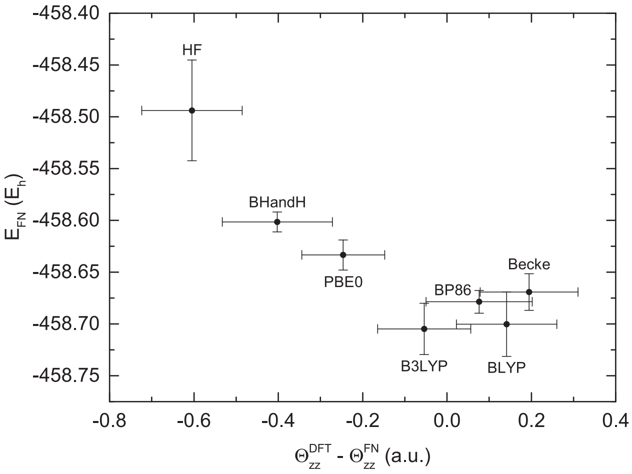

Figure 10. Fixed-node energy for bifuran ground-state versus error in the *zz*-component of the quadrupole moment tensor. Energy-optimised geometry, where the molecule rests in the *xy*-plane, and *y* is the long axis of the molecule. Coordinate origin is taken in the molecular plane at the middle of the molecule's long and short axes. The *z*-axis is perpendicular to the molecular plane. The two furan rings are in the *anti* confirmation. The dipole moment vanishes by symmetry (point group C_{2h}).

Upon subtracting the fixed-node *zz*-component of the electric quadrupole moment from its DFT-calculated value, the resulting error in the π-electron density converges to that of the best set of functionals as the fixed-node energy decreases (Figure 10).

5. Summary and conclusions

As evidenced by the quality of their fixed-node energies, the best wave functions for ethylene and bifuran have no more than 27% exact exchange, showing definitely that lowering exchange is better.

While sampling in ethylene's molecular plane, all density functional models fail to agree with quadrupole moment components calculated by coupled cluster methods.

DFT wave functions with zero exact exchange are guaranteed to obey the tiling property [68] (as does the fully correlated ground state wave function), while the HF wave function is not. Our best wave function of this type for ethylene, BP86 (with one parameter), performs comparable to M06 (with several parameters), the best one with non-zero exact exchange. BP86 is also among the functionals that are accurate both in π-electron density and energy for bifuran. This gives one hope that the 'correct reasons for success' [5] in the field of density functional theory rest with this and similar, non-empirical models.

Except for the fixed-node approximation, which is believed to be small, our calculations are free from the biases and approximations inherent in other quantum Monte Carlo approaches. Additionally, they are all-electron, thereby avoiding pseudo-potential error as well. Regrettably, calculations performed to this amount of rigour are a factor of 10^3 more expensive than standard quantum chemistry calculations. For this reason, future work of this nature aimed at choosing suitable density functionals for large extended π-electron systems would necessarily require the use of pseudo-potentals.

Acknowledgments

The authors thank Compute Canada for giving us access to their high-performance computing facilities at SHARCNET. We gratefully acknowledge Ajhit Perera's sharing with us the results of his unpublished CCSD(T) calculations on ethylene. Valuable guidance for this work was provided by Ulrike Salzner. Stuart Rothstein acknowledges hospitality afforded to him when a visitor to Hebrew and Bilkent Universities and a participant at the 58th Sanibel Symposium. Roi Baer gratefully acknowledges the support from the US-Israel Binational Science Foundation [grant number BSF-2015687].

Disclosure statement

No potential conflict of interest was reported by the authors.

ORCID

Stuart M. Rothstein http://orcid.org/0000-0002-0583-8625
Roi Baer http://orcid.org/0000-0001-8432-1925

References

[1] M.G. Medvedev, I.S. Bushmarinov, J. Sun, J.P. Perdew and K.A. Lyssenko, Science **355** (6320), 49 (2017).
[2] K.P. Kepp, Science **356** (6337), 496b (2017).
[3] M.G. Medvedev, I.S. Bushmarinov, J. Sun, J.P. Perdew and K.A. Lyssenko, Science **356** (6337), 496c (2017).
[4] P.D. Mezei, G.I. Csonka and K. Mihaly, J. Chem. Theory Comput. **13**, 4753 (2017).
[5] S. Hammes-Schiffer, Science **355** (6320), 28 (2017).
[6] K.R. Brorsen, Y. Yang, M.V. Pak and S. Hammes-Schiffer, J. Phys. Chem. Lett. **8**, 2076 (2017).
[7] M. Korth, Angew. Chem. Int. Ed. **56**, 5396 (2017).
[8] Y. Zhao and D.G. Truhlar, Theor. Chem. Acc. **120**, 215 (2008).
[9] E. Ospadov and S.M. Rothstein, J. Chem. Phys. **142**, 024114 (2015).
[10] J. Vrbik, E. Ospadov and S.M. Rothstein, J. Chem. Phys. **145**, 026101 (2016).
[11] J.B. Anderson, J. Chem. Phys. **65**, 4121 (1976).
[12] F. Mentch and J. Anderson, J. Chem. Phys. **74**, 6307 (1981).
[13] P.J. Reynolds, D.M. Ceperley, B.J. Alder and W.A. Lester, Jr., J. Chem. Phys. **77**, 5593 (1982).
[14] S. Baroni and S. Moroni, Phys. Rev. Lett. **82**, 4745 (1999).
[15] S. Baroni and S. Moroni, in *Proceedings of the NATO Advanced Study Institute, Ithaca, New York*, edited by M.P. Nightingale and C.J. Umrigar (Quantum Monte Carlo Methods in Physics and Chemistry, 1999), Vol. 525, pp. 313–341.
[16] C. Pierleoni and D.M. Ceperley, Chem. Phys. Chem. **6**, 1872 (2005).
[17] S.M. Rothstein, Can. J. Chem. **91**, 505 (2013).
[18] L. Mitas and J. Kolorenc, in *Theoretical and Computational Methods in Mineral Physics: Geophysical Applications*, edited by R. Wentzcovitch and L. Stixrude (Reviews in Mineralogy and Geochemistry, Mineralogical Society of America, Chantilly, VA, 2010), Vol. 71, Chap. 7, pp. 137–145.
[19] M. Caffarel, E. Giner, A. Scemama and A. Ramirez-Solis, J. Chem. Theory Comput. **10**, 5286 (2014).
[20] L. Wagner and L. Mitas, Chem. Phys. Lett. **370**, 412 (2003).
[21] N.A. Benedek, I.K. Snook, M.D. Towler and R.J. Needs, J. Chem. Phys. **125**, 104302 (2006).
[22] L.K. Wagner and L. Mitas, J. Chem. Phys. **126**, 034105 (2007).
[23] Y. Kanai and J.C. Grossman, Phys. Rev. A **80**, 032504 (2009).
[24] E. Sola, J.P. Brodholt and D. Alfe, Phys. Rev. B **79**, 024107 (2009).
[25] J. Ma, D. Alfe, A. Michaelides and E. Wang, J. Chem. Phys. **130**, 154303 (2009).
[26] J. Kolorenc, S. Hu and L. Mitas, Phys. Rev. B **82**, 115108 (2010).
[27] M. Korth, S. Grimme and M.D. Towler, J. Phys. Chem. A **115**, 11734 (2011).
[28] X. Jiang, X. Cheng, G. Chen and H. Zhang, Int. J. Quantum Chem. **112**, 2627 (2012).
[29] A. Ambrosetti, D. Alfe, R.A. DiStasio, Jr. and A. Tkatchenko, J. Phys. Chem. Lett. **5**, 849 (2014).
[30] M. Dubecky, R. Derian, P. Jurecka, L. Mitas, P. Hobza and M. Otyepka, Phys. Chem. Chem. Phys. **16**, 20915 (2014).
[31] K. Hongo, M.A. Watson, T. Iitaka, A. Aspuru-Guzik and R. Maezono, J. Chem. Theory Comput. **11**, 907 (2015).
[32] R.C. Clay, M. Holzmann, III, D.M. Ceperley and M.A. Morales, Phys. Rev. B **93**, 035121 (2016).
[33] M.C. Per, K.A. Walker and S.P. Russo, J. Chem. Theory Comput. **8**, 2255 (2012).
[34] D.M. Cleland and M.C. Per, J. Chem. Phys. **144**, 124108 (2016).
[35] P.A. Whitlock, D.M. Ceperley, G.V. Chester and M.H. Kalos, Phys. Rev. B **19**, 5598 (1979).
[36] I.G. Gurtubay and R.J. Needs, J. Chem. Phys. **127**, 124306 (2007).
[37] I. Kylanpaa, J. Balachandran, P. Ganesh, O. Heinonen, P.R.C. Kent and J.T. Krogel, PR Mater. **1**, 065408 (2017).

[38] Y. Yao and Y. Kanai, Chem. Phys. Lett. **618**, 236 (2015).

[39] D.M. Ceperley and M.H. Kalos, in *Monte Carlo Methods in Statistical Physics*, edited by K. Binder, Vol. 7 (Springer, Berlin, 1979), p. 145.

[40] W.K. Yuen and S.M. Rothstein, in *Advances in the Theory of Quantum Systems in Chemistry and Physics*, edited by P.E. Hoggan, E.J. Brändas, J. Maruani, P. Piecuch and G. Delgado-Barrio, *Progress in Theoretical Chemistry and Physics*, Vol. 22 (Springer, Dordrecht, 2012), pp. 327–342.

[41] S. Sorella, M. Casula, L. Spanu and A. Dal Corso, Phys. Rev. B **83**, 075119 (2011).

[42] L.K. Wagner, Int. J. Quantum Chem. **114**, 94 (2014).

[43] K. Doblhoff-Dier, J. Meyer, P.E. Hoggan, G.J. Kroes and L.K. Wagner, J. Chem. Theory Comput.**12**, 2583 (2016).

[44] M.F. DePasquale, S.M. Rothstein and J. Vrbik, J. Chem. Phys. **89**, 3629 (1988).

[45] S. Rothstein and J. Vrbik, J. Chem. Phys. **87**, 1902 (1987).

[46] J. Anderson and D. Garmer, J. Chem. Phys. **87**, 1903 (1987).

[47] P. Reynolds, R. Owen and W. Lester, J. Chem. Phys. **87**, 1905 (1987).

[48] G. te Velde, F.M. Bickelhaupt, E.J. Baerends, C. Fonseca Guerra, S.J.A. van Gisbergen, J.G. Snijders and T. Ziegler, J. Comput. Chem. **22**, 931 (2001).

[49] C. Fonseca Guerra, J.G. Snijders, G. te Velde and E.J. Baerends, Theor. Chem. Acc. **99**, 391 (1998).

[50] G. Herzberg, *Electronic Spectra and Electronic Structure of Polyatomic Molecules* No. III in Molecular Spectra and Molecular Structure (D. Van Nostrand Co, New York, 1966).

[51] A. Becke, J. Chem. Phys. **98**, 1372 (1993).

[52] C. Lee, W. Yang and R. Parr, Phys. Rev. B **37**, 785 (1988).

[53] J. Tao, J. Perdew, V. Staroverov and G. Scuseria, Phys. Rev. Lett. **91**, 146401 (2003).

[54] V. Staroverov, G. Scuseria, J. Tao and J. Perdew, J. Chem. Phys. **119**, 12129 (2003).

[55] V. Staroverov, G. Scuseria, J. Tao and J. Perdew, J. Chem. Phys. **121**, 11507 (2004).

[56] Y. Zhao and D.G. Truhlar, J. Chem. Phys. **125**, 194101 (2006).

[57] M. Ernzerhof and G. Scuseria, J. Chem. Phys. **110**, 5029 (1999).

[58] C. Adamo and V. Barone, J. Chem. Phys. **110**, 6158 (1999).

[59] A. Becke, J. Chem. Phys. **98**, 5648 (1993).

[60] P. Stephens, F. Devlin, C. Chabalowski and M. Frisch, J. Phys. Chem. **98**, 11623 (1994).

[61] J.P. Perdew, K. Burke and M. Ernzerhof, Phys. Rev. Lett. **77**, 3865 (1996).

[62] A. Becke, Phys. Rev. A **38**, 3098 (1988).

[63] J. Perdew, Phys. Rev. B **33**, 8822 (1986).

[64] J. Perdew, Phys. Rev. B **34**, 7406 (1986).

[65] M.A.L. Marques, M.J.T. Oliveira and T. Burnus, Comput. Phys. Commun. **183**, 2272 (2012).

[66] A. Perera, *Private Communication*.

[67] D. O'Neill and P. Gill, Mol. Phys. **103**, 763 (2005).

[68] D.M. Ceperley, J. Stat. Phys. **63**, 1237 (1991).